Frequency Regulation by the Distributed Hydrogen Storage Power Plant (HSPP)

Nayeemuddin Ahmed, Harald Weber
Electrical Energy Supply (EEV)
Institute for Electrical Power Engineering (IEE)
University of Rostock
Rostock, Germany
{nayeemuddin.ahmed, harald.weber}@uni-rostock.de

***Abstract*—The pursuit for carbon neutrality has led to a significant increase of renewable energy infeed to the electrical grid over the last few decades. High penetration of such intermittent sources has made it difficult for system operators to ensure grid stability in terms of frequency, voltage and power quality. The operation of stochastic renewable resources over different timescales has increased the dispatch of emergency power reserves in some situations and led to power curtailment in others. Both of these processes have resulted in a significant loss of revenue for the grid operator. Hence, to improve power system flexibility, a large-scale energy storage scheme is required, which will help maintain a continuous balance between electrical power generation and consumption, minimizing associated penalties. The Hydrogen Storage Power Plant (HSPP) is one such solution. Such an interconnected system has been designed to not only mitigate the randomness in power generation due to renewables but also provide crucial frequency (synthetic inertia) and voltage ancillary support to the grid, especially in the absence of fossil-fired power plants in the future.**

In this paper, a novel structure of the HSPP consisting of storages and DC-AC converters (HSPP-AC) is proposed. Under this renewed structure, the power plant can be operated as one unit (Combined HSPP-AC) as well as split into individual storages and converters (Distributed HSPP-AC). Distributed HSPP-AC operation would make it easier to choose optimized locations of the power plant components and lead to an easier scale-up process. This research is aimed to test the behavior of this Distributed HSPP-AC structure against its combined form as well as other types of power plants. This is achieved by implementing both HSPP variations in an isolated network containing conventional thermal and hydroelectric as well as a large share of wind power plants. The dynamic interaction of the different HSPP-AC versions with the other power plants and the roles of their internal components are analyzed in response to electrical disturbances in the three-phase grid. The results are expected to signify that the Distributed HSPP-AC, just like its combined counterpart, can ensure stable operation of a grid with a high penetration of renewable sources.

I. Introduction

Due to the stochastic nature of electrical energy generation from RES and consumption by loads, at times there is either an energy deficit or surplus in the grid. This is balanced mostly by conventional coal power plants which run on fossil fuels. However, with Germany's planned shutdown of all such power plants in the future, the number of synchronous machines in the electrical grid would drastically reduce. This will additionally lower the rotational inertia in the grid which is inherently responsible for grid stability [1], [2], [3]. To compensate for the intermittent and decentralized RES, large scale Electrical Energy Storage (EES) systems are viable alternatives [4]. Additionally, an innovative system is required which can provide the same ancillary services and ensure reliability in electrical grids as accomplished by coal power plants at present. Such a hybrid interconnected system is presented in this paper and is called the Hydrogen Storage Power Plant (HSPP) [5].

Currently, there are two main versions of the HSPP. One consists primarily of storages and DC-DC converters (HSPP-DC). The frequency ancillary service provided by this type of the HSPP has been discussed before [6], [7]. However, this paper includes a novel version of the HSPP consisting of storages and mainly DC-AC converters (HSPP-AC). The structural design of the HSPP-AC offers more flexibility when it comes to its implementation. The power plant's constituent storages and converters can be connected together to form one complete system (Combined HSPP-AC). Alternatively, the HSPP-AC can also be split into its individual storages and converters (Distributed HSPP-AC). Infact, the latter version seems to be more preferable to the German Transmission System Operators (TSOs) and other major companies associated with the power industry [8], [9]. Hence, this paper investigates the dynamic frequency regulation by the Distributed HSPP-AC in relation to its combined version and other types of power plants.

The next section briefly describes the working principle of the two HSPP-ACs. This is followed by the description of the test grid. The associated results which describe the detailed performance of the Distributed HSPP-AC is included in Section IV. Finally the research highlights are presented in the conclusion.

II. Internal HSPP Structure

The two state of the art HSPP forms are presented in Fig. 1. In such power plants, following a sudden change in power demand or generation at the three-phase network, the tasks of providing instantaneous reserve (IR), primary and secondary control power are accomplished by its three main storages; supercapacitor, battery and hydrogen storage respectively [7], [10], [11]. These three storages have different capacities and specific characteristics which make them ideal components to fulfill their respective tasks. The HSPP-DC, shown in Fig. 1a, consists mainly of these three storages and DC-DC converters. The power plant is modeled in such a way that the respective DC-DC converters control the power transfer via the current flow between adjacent storages. Since the internal components in the HSPP-DC operate in DC

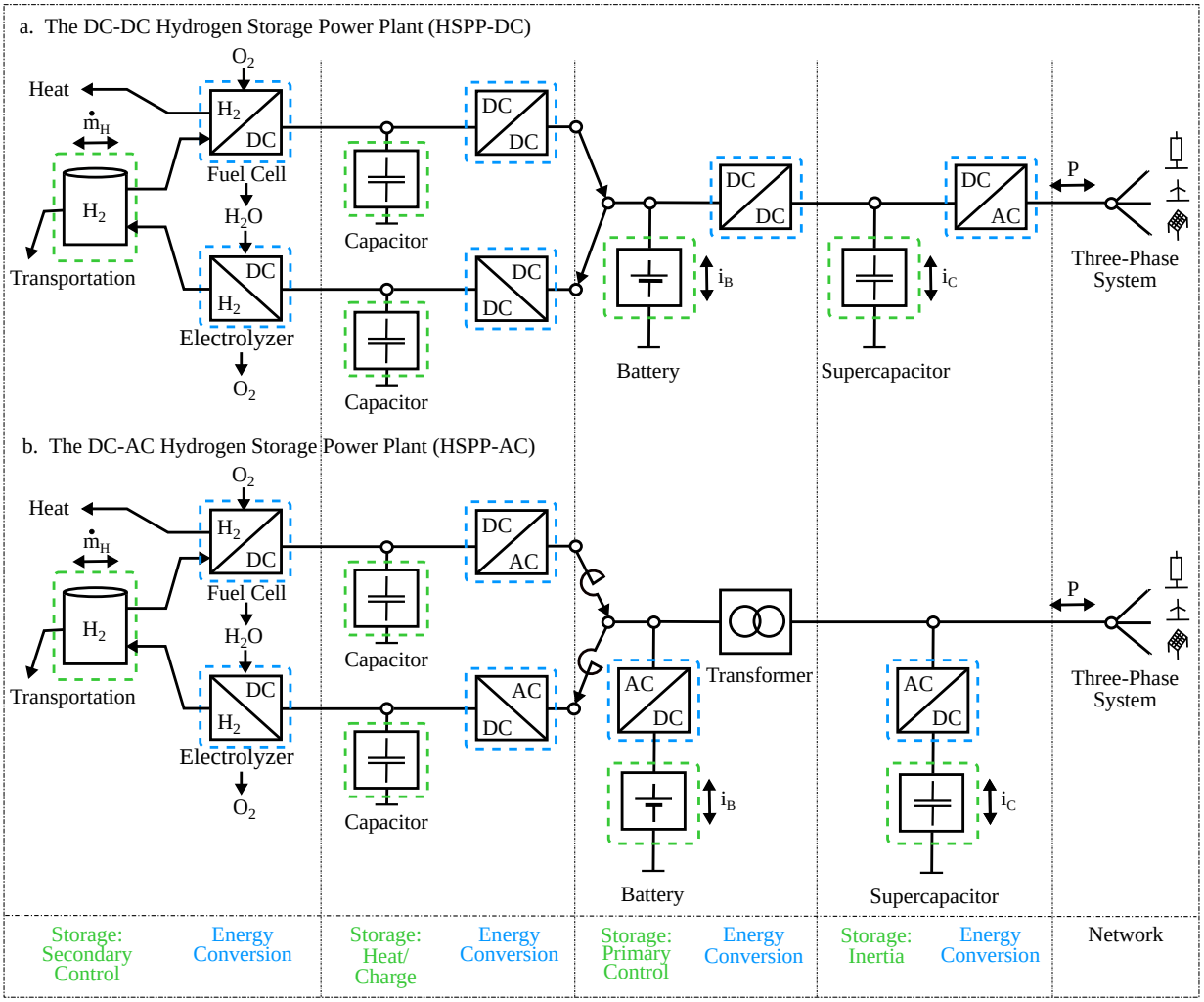

Fig. 1. Comparison between the technical structures of a) HSPP-DC and b) HSPP-AC power plant

mode, the power plant requires a DC-AC converter for grid connection.

Though the HSPP-AC uses the same three primary storages as its DC counterpart, this power plant uses DC-AC converters, which control the power transfer depending on the voltage level of these storages. It uses a supercapacitor to provide IR, since the component can charge and discharge instantaneously with a high power gradient in response to network disturbances. In addition, its ability to withstand frequent charging and discharging makes it an ideal device for inertia emulation [8].

The voltage of the supercapacitor is controlled to govern the primary control power flow from the battery using the adjacent DC-AC converter. In contrast to the supercapacitor, the battery is suited for this task since it is a cheaper form of storage with a higher energy density, enabling it to supply power for a longer duration [12]. Rapid charging or discharging of the battery is detrimental to its average lifetime and as a result, use of battery systems for providing IR is still unproven [13]. Hence, the combination of the supercapacitor in parallel to the battery ensures the required IR and primary control provisions. Additionally, a transformer is placed between the two parallel branches to protect the battery and other internal components of the HSPP-AC from electrical transients.

Both forms of the HSPP are bidirectional in nature, i.e. they can provide or store electrical energy depending on the power flow direction in the grid. The third main storage in the HSPP-AC, i.e. the hydrogen storage, is hence responsible for supplying or absorbing secondary control power. Depending on the power flow direction, either a fuel cell or an electrolyser can be used to unload or load the hydrogen storage. The power flow for each of these cases is controlled by the DC-AC converter in the respective paths between the hydrogen storage and the battery. Each of these converters are connected to series reactors to dampen the transients reaching the fuel cell and electrolyser.

While utilizing the hydrogen storage, the fuel cell generates electrical energy via the chemical reaction between stored hydrogen (H_2) and external oxygen (O_2). The reaction is exothermic and the resulting thermal energy can be used for district heating. Water (H_2O), also produced due to the reaction, can serve as the electrolyte in case of a reversed power flow, i.e. surplus power feed-in from the grid. The hydrogen produced via electrolysis can be stored in a Liquid Organic Hydrogen Carrier (LOHC) system. Such a system enables safe, easy storage and transportation of hydrogen at a high energy density under ambient conditions, using the

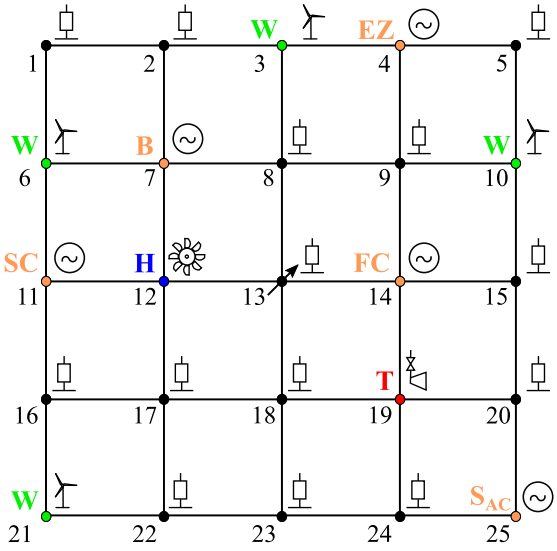

Symbol	Label	Description
	-	Load
	T	Thermal Power Plant
	H	Hydroelectric Power Plant
	W	Wind Power Plant
	S_{AC}	HSPP-AC
	SC	Supercapacitor, HSPP-AC
	B	Battery, HSPP-AC
	FC	Fuel Cell, HSPP-AC
	EZ	Electrolyser, HSPP-AC

Fig. 2. Test electrical grid for the investigations

currently available infrastructure [14]. In addition to being used for electrical power generation in the HSPP, the stored hydrogen can also play a vital role in sector coupling (Power-to-X) and decarbonisation of industrial processes [15].

III. Test Electrical Network

The network used for the investigations is shown in Fig. 2. It consists of 25 equidistant nodes, each connected to either a power plant or a load. The nodes are interconnected via transmission lines, each 250 km long and at a voltage level of 110 kV. The line impedances are equal in magnitude with a resistance to reactance ratio of 0.1. This is a generalized grid structure that has been used for multiple research studies (including voltage-reactive power control). The purpose was to create a weak network and show that HSPPs function efficiently even under such conditions.

As can be observed in Fig. 2, the network contains both the Combined HSPP-AC and Distributed versions of the HSPP-AC. The Combined HSPP-AC unit is present in node 25. This means that the entire structure described in Fig. 1 is located at that particular node. The Distributed HSPP-AC components consist of the supercapacitor, battery, fuel cell and electrolyser at the nodes 11, 7, 14, and 4 respectively. There are six other power plants, of which four are wind power plants (W) while the other two each denote

TABLE I
Initial Working Points of the Different Power Plants and Loads

Type	No.	Power per PP (MW)	Total power (MW)
Thermal power plant	1	6	6
Hydro power plant	1	6.036	6.036
Wind power plant	4	4	16
HSPP-AC Combined	1	0	0
Supercapacitor	1	0	0
Battery	1	0	0
Fuel Cell	1	0	0
Electrolyser	1	0	0
Total generation	-	-	**28.036**
Load	14	2	28
Losses	-	-	0.036
Total consumption	-	-	**28.036**

a conventional hydroelectric (H) and a coal fired thermal (T) power plant. The remaining 14 nodes, each house a load.

The network modelling and RMS simulations are performed in the software DIgSILENT PowerFactory. The initial load flow setpoints for the different types power plants are summarized in Table I. This denotes the initial conditions for the RMS simulations which will exhibit the dynamic frequency regulating behavior of the respective power plants. The HSPP-AC versions are also linked to a centralized Automatic Generation Controller (AGC). Hence only these power plants are responsible for carrying out the role of secondary control in the grid.

IV. Results and Observations

To analyze the dynamic behavior of the Combined HSPP-AC against its Distributed version and other power plants, a step increase in power consumption is implemented at the central load in the test grid. Hence, at 50s, the power demand of the load at node 13 increases by 10% (2.8 MW) of the total initial grid power consumption (28 MW). This rise in demand is represented in Fig. 3a. Per unit (pu) values are used with an apparent power base (S_{base}) of 10 MVA.

This sudden increase in total power demand leads to a negative Rate of Change of Frequency (RoCoF), as explained by (1) [16]. The corresponding frequency change in pu is

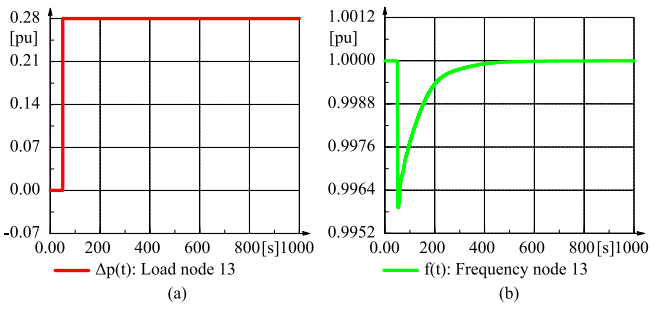

Fig. 3. (a) Active power consumption increase and (b) Frequency change at load node 13

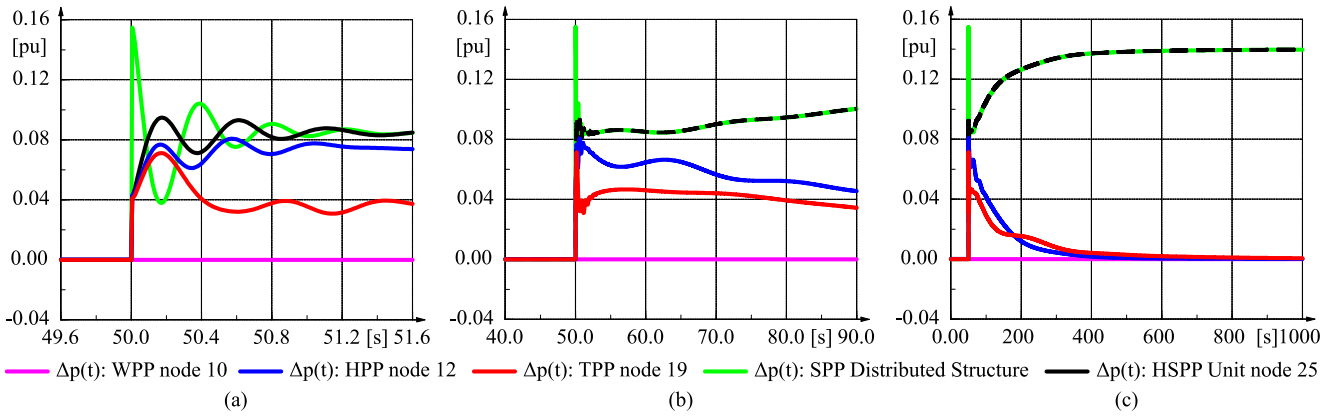

Fig. 4. Active power output of the 5 different power plant types during a) Short, b) Medium and c) Long time frame

displayed in Fig. 3b. The magnitude of this initial RoCoF depends on the size of the disturbance as well as the acceleration time constant which is a representative of the power system inertia. The frequency reduction is halted by the onset of primary controller action in the different power plants present in the grid. Afterwards, the AGC present only in the two versions of the HSPP restores the frequency to its initial set point of 1 pu.

$$\mathrm{RoCoF} = \frac{\mathrm{df}}{\mathrm{dt}} = \frac{1}{\mathrm{T_a}} \cdot (\mathrm{p_G} - \mathrm{p_L}) \tag{1}$$

where:

$\frac{\mathrm{df}}{\mathrm{dt}}$	First order time derivative of frequency (pu)
$\mathrm{T_a}$	Acceleration time constant (s)
$\mathrm{p_G}$	Total active power generated (pu)
$\mathrm{p_L}$	Total active power consumed (pu)

To meet the increase in power demand, some of the power plants present in the grid correspondingly increase their active power outputs. Fig. 4 exhibits this change for the different power plant types over three different time scales. The instantaneous response of the power plants, present in Fig. 4a, shows that the Distributed HSPP-AC provides a greater initial power increase than its counterparts. This is because the output of the Distributed HSPP-AC is the sum of the individual responses from its components (i.e. the supercapacitor, battery, fuel cell and electrolyser at nodes 11, 7, 14 and 4 respectively). Since the electrical distance between three of these components (supercapacitor, battery and fuel cell) and node 13 is quite low, the response of each element is quite significant, which sum to a higher power output for the Distributed HSPP-AC.

The instantaneous response of the thermal and hydro power plants stem from the inertia of their turbine-generator shaft. For the thermal plant, the steam pressure reduces after its initial response. This leads to a reduction in its power output. The Combined HSPP-AC at node 25 is farthest from the source of disturbance amongst the power plants. Due to high impedance of the connecting path, the response from its synthetic inertia is lower than the Distributed HSPP-AC but comparable that of the conventional plants. The Wind Power Plants (WPPs) are represented by simplified converters operating at their Maximum Power Point (MPP). Hence, they do not show any increase in their power output.

Fig. 4b shows the variation of power plant outputs under the action of the primary controller. The thermal plant momentarily increases its output power due to the opening of the steam valve which restores the steam pressure. However, after a short period, the maximum valve position is reached and the steam pressure reduces again leading to further decrease in the power output. The Hydroelectric Power Plant (HPP) also shows a gradual decrease in its power output owing to the loss of water pressure in the long penstock. The two versions of the HSPP-AC display the same increase in power output due to possessing identical power-frequency droop characteristics.

During this time, the secondary controller action (AGC) starts to gradually come into effect. Since the AGC is only present in the two versions of the HSPP-AC, the output power of these two plants rise, while the other power plants return to their original power set points, as shown in Fig. 4c. The participation factor of both HSPP-AC versions in the AGC structure is 0.5. Hence, they have identical final power outputs. The sum of these two power increases is just above 0.28 pu and is used to satisfy the increased load demand and associated negligible power losses in the system.

Fig. 5a shows the instantaneous response provided from the three main storages of the Distributed HSPP-AC. About 60% of this immediate response originates from the supercapacitor and 15% from the battery. The rest is provided by the fuel cell and electrolyzer via the hydrogen storage. The plot for the hydrogen mass flow rate to the electrolyzer is not included since it largely overlaps with the mass flow rate to the fuel cell in Fig. 5a, b and then then remains at 0 during the steady state. As stated earlier, the control mechanism of the HSPP-AC has been designed so that the supercapacitor provides the required instantaneous response. However, since the disturbance is at node 13, the fuel cell is closer to this point while the supercapacitor and battery are equidistant from it. Due to the lower impedance between node 13 and the fuel cell compared to that with the supercapacitor, part of the initial response originates from the hydrogen storage linked to the fuel cell. The same reason holds for the initial response of the battery. The peak initial battery current and

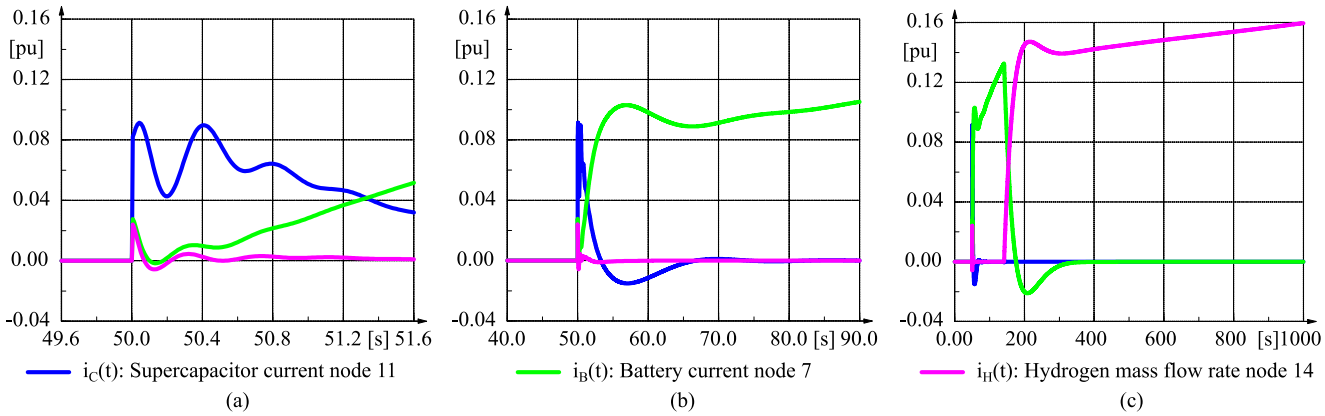

Fig. 5. Response from the Distributed HSPP-AC storages during a) Short, b) Medium and c) Long time frame

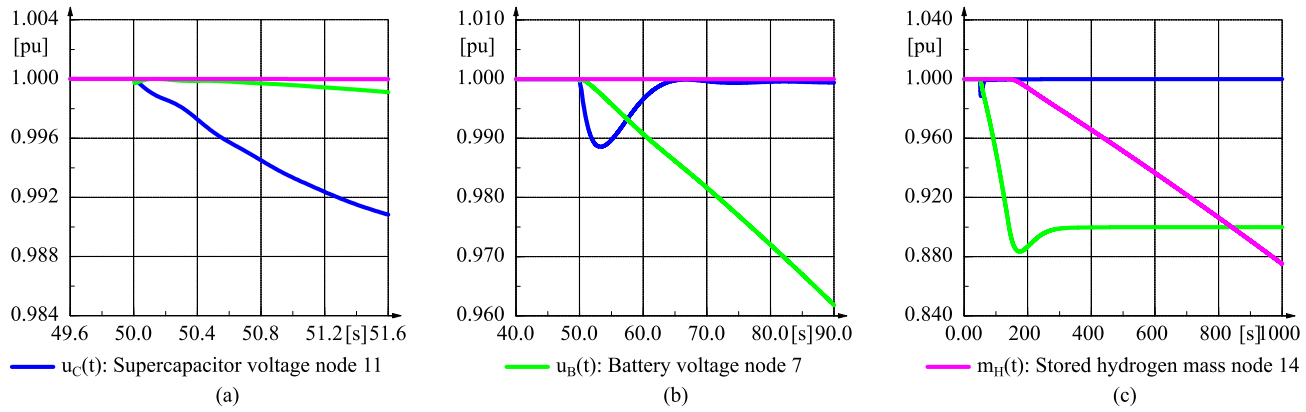

Fig. 6. Energy levels of the Distributed HSPP-AC storages during a) Short, b) Medium and c) Long time frame

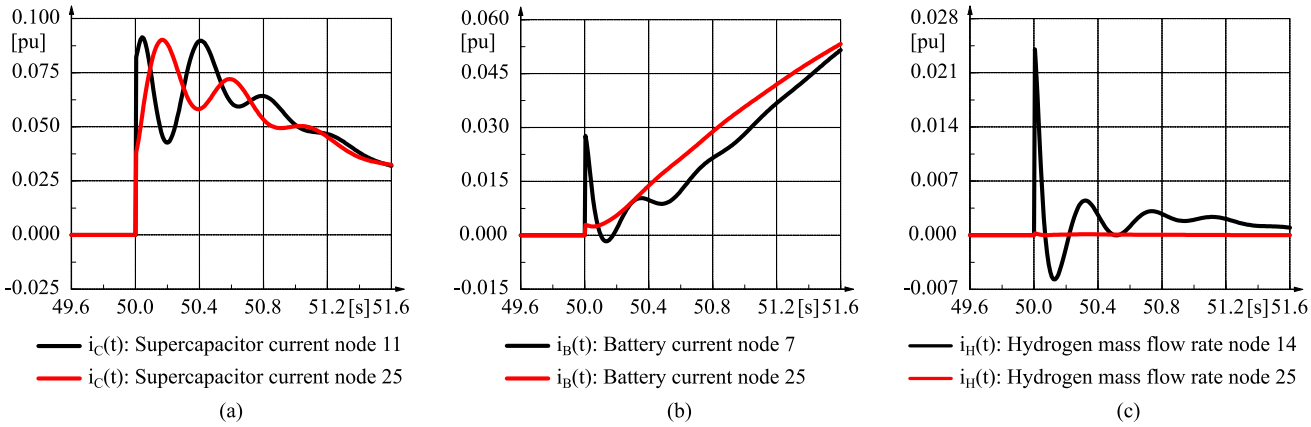

Fig. 7. Comparison between the outputs of the two different HSPP-AC versions during the short time frame

mass flow rate to the fuel cell can be reduced by increasing their connecting impedances to the grid. However, this also introduces the additional drawback that the post disturbance residual current from these storages persists longer.

Fig. 5b presents the response from the same storages over the medium timescale. After the initial momentary spike, both hydrogen mass flow rates to the fuel cell and elecrolyzer return to 0. The supercapacitor discharges upon providing the largest share of the instantaneous reserve, as shown in Fig. 6a, and is then recharged by the battery. This recharging phase is shown in Fig. 5b, by the negative supercapacitor current, and Fig. 6b by the supercapacitor voltage being returned to its set point of 1 pu. The action of the battery represents the onset of the primary control power. During the medium time frame, the battery alone recharges the supercapacitor and produces the required active power for the Distributed HSPP-AC to meet the increased demand.

Providing primary control power over an extended time period causes the battery to discharge as well. Once its voltage surpasses the lower threshold of 0.9 pu, as shown in Fig. 6c, the fuel cell is triggered into action. The hydrogen storage increases the rate of hydrogen input to the fuel cell, as displayed in Fig. 5c, causing it to produce more power. This secondary control power flow from the hydrogen

storage is used to recharge the battery, i.e. return the battery voltage within permissible thresholds, and meet the increased power demand. The magnitude of this secondary control power is regulated in the centralized AGC.

Equation (2) links the power output of the Distributed HSPP-AC, presented in Fig. 4, with the current and voltage levels in the storages shown in Fig. 5 and 6. The figure legends describe the quantities used in the equation.

$$\Delta p(t) = i_c(t) \cdot u_c(t) + i_B(t) \cdot u_B(t) + i_H(t) \cdot m_H(t) \quad (2)$$

Fig. 7a compares the current output from the respective supercapacitors of the two HSPP-AC versions. Since the supercapacitor for the Distributed HSPP-AC is located much closer to node 13 compared to the one in the Combined HSPP-AC, the instantaneous response provided by the former storage is higher. However, about 1.2 s after the inception of the disturbance, the current output from both storages become equal since the required instantaneous provisions are met. Both currents are then gradually restored to 0. The battery at node 7 is also much closer to node 13 compared to node 25, causing it to output a higher initial current, shown in Fig. 7b. In addition, the presence of an extra transformer between the supercapacitor and battery for the Combined HSPP-AC at node 25, further increases the impedance of the connecting path and lowers the initial shock on the battery. As in the previous case with the two supercapacitors, the battery currents also reach the same value after a few seconds since both HSPP-AC versions provide the same primary control power, exhibited in Fig. 4b.

The biggest difference is observed for the hydrogen mass flow rates to the two respective fuel cells in Fig. 7c. Since the fuel cell for the Distributed HSPP-AC is located adjacent to node 13, the low impedance of this connecting path activates an initial spike in the rate of hydrogen mass flow. A similar peak of a slightly lower magnitude is also observed for the mass flow rate to the electrolyzer at node 4. However, after this initial peak, the hydrogen mass flow rates both at nodes 4 and 14 quickly return to 0 till the fuel cell is activated again around 150 s, Fig. 5c. Conversely the fuel cell and electrolyser in the Combined HSPP-AC at node 25 is well protected from this initial jolt due to its connecting reactor coils and transformer, Fig. 1. As a result, the instantaneous hydrogen mass flow to both of these components is negligible.

The behavior of the Distributed and Combined HSPP-AC versions are very similar except for their respective instantaneous responses. Based on this initial behavior the Combined HSPP-AC proves to be a more technically proficient solution. However, if this issue does not play a significant role, then the Distributed HSPP-AC will be the preferred alternative due to its scalability and associated economic profitability.

V. Conclusion

This paper exhibited the ability of two different versions of the HSPP-AC to function effectively with conventional plants and renewable resources in a 25 node frequency controlled grid. Inside this network, a disturbance was created by implementing a step increase in the power consumption by the load at node 13. The corresponding dynamic responses of the conventional plants and HSPP-AC versions were analyzed. It was shown that both forms of the HSPP-AC are able to provide the necessary ancillary response in the form of instantaneous reserve, primary and secondary control to overcome the disturbance. The primary difference between the Distributed and Combined HSPP-AC was recognized to be in the provision of their instantaneous response.

Details regarding the control scheme of the HSPP are present in [17]. The efficiency, power ratings and relative storage sizes are currently under discussion for a 10 MW HSPP and will be discussed in future publications. Further research will also be required to model the processes inside the electrolyser and fuel cell in greater detail. This will help to estimate the total system losses as well as the market compatibility of this novel scheme.

References

[1] German Institute for Economic Research, *Phasing out Coal in the German Energy Sector*. DIW Berlin, 2019.

[2] X. Liang, "Emerging power quality challenges due to integration of renewable energy sources," *IEEE Transactions on Industry Applications*, vol. 53, no. 2, pp. 855–866, 2016.

[3] G. Chown, J. G. Wright, R. P. Van Heerden, and M. Coker, "System inertia and rate of change of frequency (rocof) with increasing non-synchronous renewable energy penetration," 2017.

[4] A. Othman and H. Gabbar, "Energy storage integration within interconnected micro energy grids," in *Smart Energy Grid Engineering*. Elsevier, 2017, pp. 207–220.

[5] H. Weber, "Von der frequenzregelung mit schwungmassen (netzstützende maßnahmen) zur winkelregelung mit umrichtern (netzbildende maßnahmen), from frequency control with inertia to angle control with converters," 2017.

[6] H. Weber, "The ancillary response of storage power plants in the present and future electrical grid," in *Energy Transition in Power Supply - System Stability and System Security; 13th ETG/GMA-Symposium*, 2019.

[7] P. Gerdun, N. Ahmed, V. Vernekar, M. Töpfer, and H. Weber, "Dynamic operation of a storage power plant (spp) with voltage angle control as ancillary service," in *2019 International Conference on Smart Energy Systems and Technologies (SEST)*. IEEE, 2019, pp. 1–6.

[8] R. Zhang, J. Fang, and Y. Tang, "Inertia emulation through supercapacitor energy storage systems," in *2019 10th International Conference on Power Electronics and ECCE Asia (ICPE 2019-ECCE Asia)*. IEEE, 2019, pp. 1365–1370.

[9] S. Kharel and B. Shabani, "Hydrogen as a long-term large-scale energy storage solution to support renewables," *Energies*, vol. 11, no. 10, p. 2825, 2018.

[10] H. Weber, N. Ahmed, M. Töpfer, P. Gerdun, and V. Vernekar, "Dynamic behavior of conventional and storage power plants in a single power system," in *2019 IEEE Milan PowerTech*. IEEE, 2019, pp. 1–6.

[11] M. Töpfer, N. Ahmed, and H. Weber, "Dimensioning the internal components of a hydrogen storage power plant," in *2020 International Conference on Smart Energy Systems and Technologies (SEST)*. IEEE, 2020, pp. 1–6.

[12] C. Brivio, S. Mandelli, and M. Merlo, "Battery energy storage system for primary control reserve and energy arbitrage," *Sustainable Energy, Grids and Networks*, vol. 6, pp. 152–165, 2016.

[13] M. G. Dozein and P. Mancarella, "Frequency response capabilities of utility-scale battery energy storage systems, with application to the august 2018 separation event in australia," in *2019 9th International Conference on Power and Energy Systems (ICPES)*. IEEE, 2019, pp. 1–6.

[14] D. Teichmann, W. Arlt, P. Wasserscheid, and R. Freymann, "A future energy supply based on liquid organic hydrogen carriers (LOHC)," *Energy & Environmental Science*, vol. 4, no. 8, pp. 2767–2773, 2011.

[15] Federal Ministry for Economic Affairs and Energy, Germany. (2020) The national hydrogen strategy. [Online]. Available: https://www.bmbf.de/files/bmwi_Nationale%20Wasserstoffstrategie_Eng_s01.pdf

[16] P. S. Kundur, N. J. Balu, and M. G. Lauby, "Power system dynamics and stability," *Power System Stability and Control*, vol. 3, 2017.

[17] Prof. Dr.-Ing. Harald Weber, "External and internal control of a storage power plant operating without rotating masses, Verfahren zur exteren und internen Regelung eines schwungmasselosen Speicherkraftwerks," Patent number: **10 2019 124 268.1**.